Tuning zeolite properties for highly efficient synthesis of propylene from methanol

Ana Palčić,[a,b] Vitaly V. Ordomsky,[c]* Zhengxing Qin,[a] Veselina Georgieva,[a] Valentin Valtchev,[a,d]*

[a]ENSICAEN, UNICAEN, CNRS, Laboratoire Catalyse et Spectrochimie, Boulevard Maréchal Juin 6, 14000 Caen, France.

[b]Ruđer Bošković Institute, Bijenička 54, 10000 Zagreb, Croatia.

[c]Univ. Lille, CNRS, Centrale Lille, ENSCL, Univ. Artois, UMR 8181 - UCCS - Unité de Catalyse et Chimie du Solide, F-59000 Lille, France.

[d]State Key Lab of Inorganic Synthesis & Preparative Chemistry, Jilin University, Changchun 130012, China.

*Valentin.Valtchev@ensicaen.fr, Vitaly.Ordomsky@univ-lille1.fr

ABSTRACT: Series of nanosized ZSM-5 samples is synthesized at 170 °C, 150 °C, 120 °C and 100 °C. Experimental data show that the decrease of crystallization temperature leads to significant changes in zeolite properties. Crystals synthesized at 100 °C exhibit many framework defects with lower acid sites density, strength and larger external surface area. The selectivity to light olefins and the propylene-to-ethylene ratio increases as the crystallization temperature decreases. Propylene-to-ethylene ratio above 6 with the highest selectivity to propylene of 53 % is obtained over ZSM-5 catalyst prepared at 100 °C. Stability of the nanosized zeolite in MTO is also improved compared to industrial sample with similar Si/Al ratio. This catalytic performance is a result of the decrease in the acid sites density, strength and the crystals' size, providing shorter diffusion path and larger external surface area. The presence of structural defects and different external surface are of the crystals has been shown to play an important role in the MTO catalyst performance.

KEYWORDS: zeolite ZSM-5; MTO; propylene; acidity; catalyst design

1 Introduction

The design of catalysts having required performance in terms of activity and selectivity to valuable products represents nowadays one of the main issues in the heterogeneous catalysis. Zeolites are one of the most widely used solid heterogeneous catalysts due to their unique properties. Amongst the others the methanol transformations to hydrocarbons (MTH) developed in Mobil is one of the very important reactions over zeolite catalysts.[1] This process has been modified further into methanol to olefins (MTO) by UOP, methanol to propylene (MTP) by Lurgi and methanol to gasoline (MTG) by Mobil.[2-4] There are some drawbacks in the mentioned processes and further improvements are required according to the prevailing needs of the market. In the past several years there has been a significant increase of the light olefins demand and this trend continues to grow. Particularly, there is a higher market demand for propylene. To overcome this propylene shortage the existing processes are revised in order to bust the propylene selectivity.

Two zeolite catalysts are commonly applied in MTH processes: a silicoaluminophosphate with CHA-type structure (SAPO-34) and an aluminosilicate with MFI-type framework topology (ZSM-5). On account of its small pore windows and mild acid strength, SAPO-34 catalyst exhibits excellent performance in production of light olefins, but deactivates quickly due to accumulation of carbonaceous residues (coke).[5] On the other hand, the deactivation rate of ZSM-5 is significantly slower and the yield of light olefins is lower.[6] The engineering of these two catalysts is still a challenging task.

In order to enhance the light olefins yield over ZSM-5 various approaches have been employed. For instance, post-synthesis modifications were used to increase the steric constraints and to achieve a favorable density and strength of Brønsted acid sites.[7-9] In the early study of Chang et al. the ratio of propylene/ethylene (P/E) of 4.9 has been reached for the sample with SiO_2/Al_2O_3 ratio 1670.[10] In general, propylene selectivity was rising with decreasing zeolite acidity. The same effect of increase of the propylene to ethylene ratio and selectivity to light olefins has been observed by Prinz and Riekert over ZSM-5 catalysts with high Si/Al ratio.[11] At low conversion (< 70 %) the selectivity for light olefins was found to be higher for smaller crystals. Moreover, relatively more propylene is generated on smaller than on the larger crystals. In addition, smaller ZSM-5 crystals showed longer catalyst lifetime in MTG reaction.[12] Propylene selectivity of 42.2% and P/E ratio of 10 was achieved over high-silica ZSM-5 with mesopores generated by alkaline desilication.[13] Such performance has been explained by enhanced diffusion and low number of Brønsted acid sites. Likewise, propylene to ethylene ratio close to 5 was obtained over fluoride medium synthesized ZSM-5 catalyst.[14] Propylene selectivity rising from 16 to 52 % and P/E ratio from 2 to 6.5 was achieved in a series of ZSM-5 catalysts having Si/Al from 12 to 360.[15]

Modification of one of the samples by phosphorous resulted in improved propylene selectivity of 56 % and propylene to ethylene ratio 7. The effect has been ascribed to elimination of some acid sites upon P modification. Furthermore, propylene selectivity of 45 % and P/E of 16 was obtained over ZSM-5 modified by zirconium oxide and phosphoric acid.[16] Herein, the number of acid sites has increased while their strength becomes weaker. Besides, the pore size shrinks slightly. The selective production of propylene from methanol has been observed over ferrosilicate with MFI-type topology (Fe-MFI) with small crystal sizes.[17] The best propylene selectivity of 48 %, in conjunction with a high propene/ethene ratio of 11.5 has been attained.

The addressed findings demonstrate the impact of physicochemical properties of zeolite on the catalysts stability and selectivity. It was possible to obtain high selectivities, mainly by decrease of the amount of acid sites, substitution of Al for Fe or by doping of zeolite leading to decrease of the number and strength of acid sites. Zeolite doping has a positive effect, but leads to decrease of the pore volume and sometimes accelerates catalyst deactivation. Moreover, the Fe-counterpart of ZSM-5 is not stable in the presence of water. It is well established that the higher amount of acid sites and higher acid site density is often the reason of fast catalyst deactivation in MTO process.[18] Hence, the best catalyst for the synthesis of propylene from methanol on the basis of literature results would be nanosized ZSM-5 crystals with lower acid sites density. Nanocrystal ZSM-5 zeolites have been already reported as efficient catalysts in comparison with micron sized counterparts in different catalytic reactions in terms of stability and selectivity.[19-21]

Among different strategies in preparing nanosized zeolites, clear sols are most often used due to the homogeneity of the system which results in crystalline product with narrow particle size distribution.[22] Besides the gel composition the conditions of synthesis have a direct impact on the end product properties.[23,24] Reaction temperature is one of the mostly varied parameters when engineering the materials. Generally, the nucleation is favored over the crystal growth at low temperatures. In consequence, smaller crystals are obtained.[20,22,24] Lowering the reaction temperature in ZSM-5 synthesis was found to affect the crystallinity, morphology and chemical composition of zeolite crystals.[25,26] Therefore, the decrease of the zeolite synthesis temperature might provide additional opportunities for adjusting the materials properties required for a particular application.

In the present work, we study the influence of the temperature of crystallization of nanosized ZSM-5 on the materials features and subsequently its performance in the MTO reaction. The principle aim is to provide stable aluminosilicate zeolite catalyst in MTO reaction with high selectivity toward propene and therefore develop a simple strategy to design more efficient catalysts.

1 Results and Discussion

2 General characterization of zeolite samples

3 Powder X-ray diffraction patterns of synthesized solids exhibit the diffraction peaks characteristic

4 of MFI-type material (Figure 1). Slight increase in the peak intensities with rising of the synthesis

5 temperature was observed. The relative crystallinity of the samples (Table 1) was determined

6 applying method established in the literature, where the peak area in the XRD pattern of the

7 samples in the range 22-25 ° 2ϑ is compared with the peak area of the reference sample.[12,26] Herein

8 the ZSM-5(ind) sample was taken as a reference. The obtained values indicate that relative

9 crystallinity gets lower with the decrease of the synthesis temperature. Such observation is in
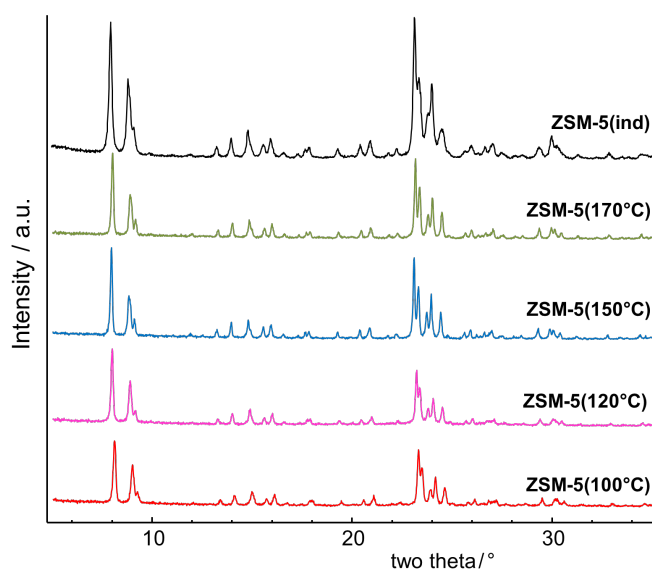

10 **Figure 1.** XRD patterns of the industrial and nanosized zeolites prepared at different crystallization

11 temperatures.

12

13 agreement with the previously reported data on both conventional and seeded synthesis of ZSM-

14 5.[26,27] The crystallinity of the samples prepared at elevated temperatures (150°C and 170°C) is

15 higher in respect to their counterparts prepared at 120°C and 100°C (Table 1).

16 Representative SEM images of the studied samples show that they exhibit the morphology typical

17 of MFI crystals, some of them having very rough surface (Figure 2). A closer look reveals that the

18 particles are composed of smaller crystallites. The TEM inspection of the ZSM-5(100°C) reveals

19 that the particles are built of randomly oriented very small crystallites resulting in corrugated

20 outline. The surface of ZSM-5(120°C) is also fairly rough due to the small size of building particles.

21 High temperature samples (150°C and 170°C) exhibit less rough surface, i.e., there are fewer
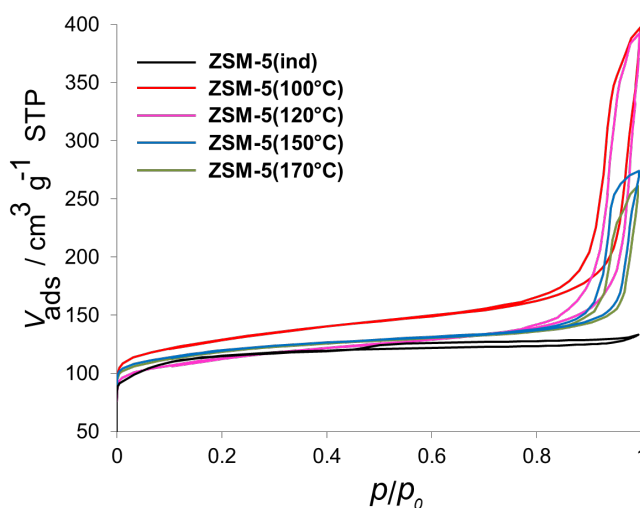
22 intergrown crystals.
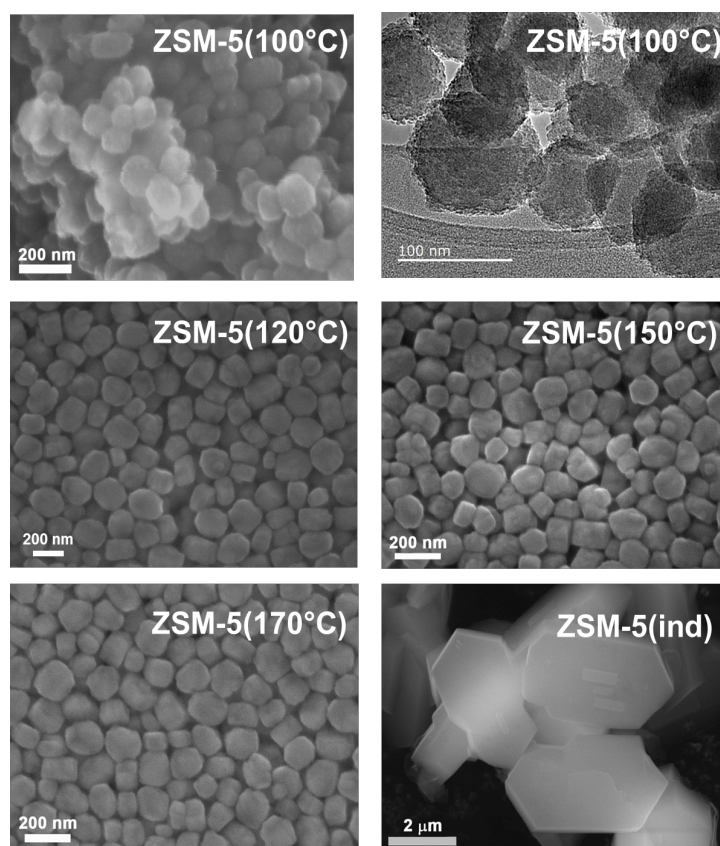
Figure 2. SEM (left) and TEM (right) micrographs of the ZSM-5(100°C) sample (the first line). SEM micrographs of the nanosized zeolites prepared at different crystallization temperatures and the industrial ZSM-5 (the second and the third line).

The particle size in each sample was determined as the average of the size of 90 measured particles (Table 1). The size of the nanosized ZSM-5 samples is ranging from 100 to 140 nm. They are getting slightly larger with increasing the synthesis temperature. As known a lower crystallization temperature favors the nucleation and thus larger number of crystallites is formed in the system, which leads to smaller ultimate particles. The reaction temperature influences also the solubility of Al and Si species and accordingly the reaction kinetics.[22,27] Consequently the concentration of reactive species in the liquid phase is inferior at lower crystallization temperature. The diffusion rate is also lower at low crystallization temperature. Combining these phenomena implies that the collisions/contacts between the reacting species is more frequent and more successful, i.e. leads to the formation of viable entities able to grow further and subsequently form a crystalline product, at a higher temperature. Briefly, at elevated temperature the growth rate is higher and the obtained crystals larger. As a result the crystallization of a particular initial system at different temperature leads to ZSM-5 particles having different levels of aggregation and crystallinity degree.

5

1 Nevertheless, all synthesized products in this study were with nanosize dimensions, much smaller

2 of the industrial sample which exhibits well shaped crystals with size 3-5 µm (Figure 2).

3

4 **Table 1.** Framework composition, size and porosity of the studied ZSM-5 samples.

Sample	Relative crystallinity %	Si/Al^{ICP}	Si/Al^{NMR}	Size nm	S_{BET} m^2g^{-1}	V_{mic} cm^3g^{-1}	S_{ext} m^2g^{-1}	V_{total} cm^3g^{-1}
ZSM-5(ind)	100	25	27	4000	377	0.180	2	0.200
ZSM-5(170°C)	86	27	36	135	391	0.175	36	0.399
ZSM-5(150°C)	87	31	35	128	389	0.177	32	0.371
ZSM-5(120°C)	72	25	37	116	388	0.147	72	0.523
ZSM-5(100°C)	71	35	46	103	428	0.142	107	0.548

5

6 **Figure 3.** Nitrogen adsorption/desorption isotherms of the industrial and nanosized zeolites

7 prepared at different crystallization temperatures.

8

9 The porosity and specific surface area of the zeolite samples were determined by nitrogen

10 adsorption/desorption measurements. The obtained isotherms are depicted in Figure 3. The

11 industrial sample, ZSM-5(ind), exhibits classical Type I adsorption isotherm with a sharp uptake at

12 low relative pressures followed by horizontal adsorption and desorption branches. On the other

13 hand, nanosized ZSM-5 samples display a mixed Type I and Type IV isotherm with a very steep and

14 almost parallel hysteresis (H1 type) in the range $p/p_0 > 0.8$. This is related to pores comprised of

15 tightly packed, nearly uniform, particles. Micropore volumes of the samples prepared at 150 and

16 170 °C are very close to those characteristic of highly crystalline MFI-type material. In contrast,

17 lower values of micropore volume of the ZSM-5(100°C) and ZSM-5(120°C) samples imply lower

18 crystallinity and the presence of certain amount of dense amorphous phase. The sample prepared at

1   120 °C shows S_{ext} 72 m^2/g, while 150 and 170 °C samples have S_{ext} of 32 m^2/g and 36 m^2/g,

2   respectively. The highest external surface area of ZSM-5(100°C) is obviously due to the smallest

3   particle size (Table 1) and rough surface which arises from very small randomly oriented crystalline

4   domains. The size of the individual crystallites building the particles can be seen on the TEM image

5   shown in Figure 2 (top, right). The sample ZSM-5(120°C) also exhibits rough surface, but the size

6   of individual crystals is larger than in the 100 °C sample. There is a significant contribution of

7   mesopores to the total pore volume of the nanosized materials, which has already been reported in

8   the literature.[28] This phenomenon is more pronounced in the samples prepared at low temperatures

9   where the crystallites are smaller. BJH analysis reveals that the size of mesopores for all studied

10   nanosized samples is in the range 20-50 nm. These relatively large pores are due to intra-particle

11   porosity.

12   **Characterization of acid sites**

13   ^{27}Al MAS NMR is a standard tool in determining the environment of aluminum atoms in zeolite

14   samples. ^{27}Al MAS NMR spectrum of fully hydrated industrial sample exhibits a sole resonance at

15   56 ppm corresponding to tetrahedrally coordinated aluminium in zeolite framework (Figure 4). The

16   spectra of nanosized samples are more complex. The peak of tetrahedrally coordinated Al is much

17   broader and asymmetric, in addition the presence of penta- (ca. 30 ppm) and octahedrally (ca. 0

18   ppm) coordinated Al is detected (Figure 4). The concentration of later species is higher in the

19   samples synthesized at 100 °C and 120 °C. In general, the integrated NMR signal intensities are

20   proportional to the number of nuclei contributing to the signal and the spectra are expected to be

21   quantitative. In spite having very similar bulk Al content (Si/Al^{ICP}) in nanosized samples (Table 1),

22   the total intensity of the signal in the spectra of zeolites crystallized at higher temperature (150 and

23   170 °C) is stronger than that the lower temperatures counterparts (100 and 120 °C). This effect

24   might be attributed to the increase of the contribution of "NMR invisible Al species" in the samples

25   prepared at lower temperatures.[29,30] The high quadrupolar moment might make their NMR signal

26   too broad and thus some species cannot be detected.

27   To get more detailed information of the exact positions of the peaks and the contributing species,

28   the spectra were decomposed using dmfit analysis software.[31] For each sample four resonances

29   were observed. The industrial sample exhibits resonance at 56 ppm corresponding to framework

30   tetrahedral aluminum atoms. The peak shifts upfield (53 ppm) for the nanosized samples. These

31   features have been earlier explained by different siting of Al atoms in the framework T sites.[32,33]

32   The Al should be localized preferentially in the sites with low Al-O distances and T-O-T angles in

33   the case of industrial sample and less constrained positions for the nanosized zeolite samples.

34   Furthermore, a signal arising from extra-framework octahedral Al at about 0 ppm is found in all

nanosized zeolites. Octahedral Al moieties give rise to one more signal in ^{27}Al MAS NMR spectra of all synthesized samples but at different positions. Resonances at 7 and 4 ppm are detected in the samples ZSM-5(100°C) - ZSM-5(120°C) and ZSM-5(150°C) - ZSM-5(170°C), respectively. Extra-framework Al may be present in zeolites in different forms as cations or neutral species occupying various positions in the micropores.[34-36] It appears that polymeric octahedral Al species (amorphous phase) have resonances at lower field than the monomeric moieties since in a cluster the nuclei get more deshielded.[37-39] Hence, on the grounds of the positions of the signals in ^{27}Al MAS NMR spectra it can be deduced that low temperature samples (7 ppm signal) have higher content of six-fold coordinated Al species built of several Al atoms (polymerized Al species) than the samples prepared at 150 °C and 170 °C (4 ppm signal).
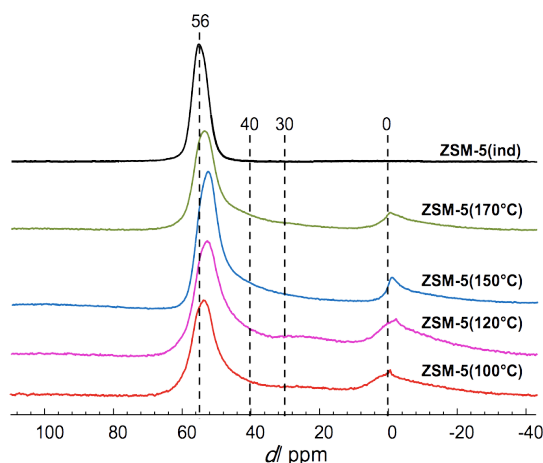

Figure 4. ^{27}Al MAS NMR spectra of the industrial and nanosized zeolites prepared at different crystallization temperatures.

In the ^{27}Al MAS NMR spectrum of each nanosized sample there is a broad signal appearing in the region 20-40 ppm. According to the spectra decomposition, in the samples ZSM-5(100°C) and ZSM-5(120°C) there is a signal at 29 ppm. On the other hand, samples ZSM-5(150°C) and ZSM-5(170°C) exhibit resonance further downfield at 38 ppm. Such large difference in the signals position indicates distinct coordination of oxygen atoms around Al species contributing to these resonances. The peaks in the 30-50 ppm region have often been found in the ^{27}Al MAS NMR spectra of MFI structure after steaming due to the partial release of framework Al atoms.[40,41] Typically perturbed four-fold coordinated or five-fold coordinated aluminium species generate signals in this region. In general, signals around 30 ppm in the ^{27}Al MAS NMR spectra are perceived to stem from extra-framework five-fold coordinated Al moieties,[42,43] while the

resonances at higher chemical shift positions emanate from less ordered framework Al atoms present in not-fully crystalline zeolites.[44] Thus, it can be concluded that the high temperature samples encompass highly distorted tetrahedral Al species (38 ppm signal) while low temperature samples involve five-fold coordinated Al (29 ppm signal). Thus the ^{27}Al NMR data indicate once again the presence of amorphous phase in the samples ZSM-5(100°C) and ZSM-5(120°C). Although less there is still a certain amount of perturbed and extra-framework Al in high temperature samples.

To further investigate the effects that occur with the decrease of the temperature of crystallization ^{29}Si MAS NMR measurements were performed (Figure 5). The main resonances appear in the range from -110 ppm to -120 ppm with two dominating signals at -113 ppm and -115 ppm. In this range there is overlapping of several signals arising from Si atoms in the nonequivalent crystallographic T positions in MFI framework. They are characteristic for Q^4 tetrahedral Si species (Si surrounded by
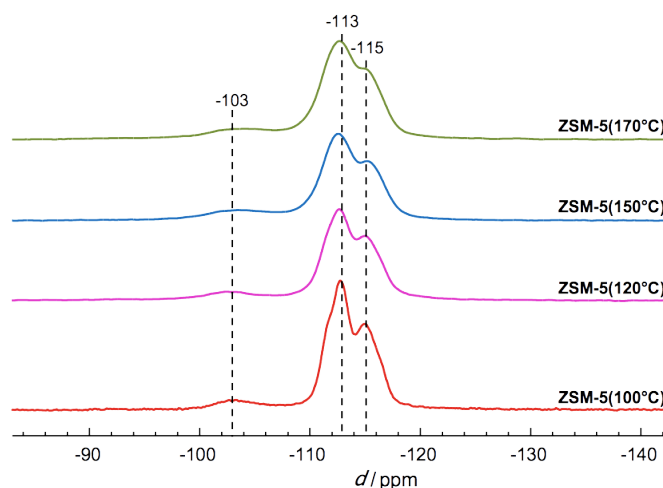

Figure 5. ^{29}Si MAS NMR spectra of the nanosized zeolites prepared at different crystallization temperatures.

four other Si atoms – Si(4Si)). Absence of resolution is caused by the presence of defects and Al in the lattice. Namely, Al prompts certain distortion of the lattice leading to change of chemical shift which depends on the distance between Al and the Q^4 Si species.[45] The band at -103 ppm is associated to Q^3 Si species, either Si(3Si, 1Al) or Si(3Si, 1OH).[46]

The [29]Si {[1]H} cross-polarization spectra plotted in Figure 6 were taken in order to study the silanol species in the samples. ^{29}Si {^{1}H} CP NMR spectra are usually not quantitative since proton-rich species are often overemphasized. Two intense resonances, at -103 ppm and -115 ppm were

1 observed in all samples. The resonance at -103 ppm is characteristic of Si(3Si, 1OH) species, while

2 the one at -115 ppm of Si(4Si) with ^{1}H in the vicinity. These data show the presence of nest type

3 silanol defects in the nanosized samples. The intensities of the resonances of Si(nAl) species in [29]Si

4 MAS NMR spectra is often used to calculate the Si/Al ratio in zeolites.[47] The main drawback of
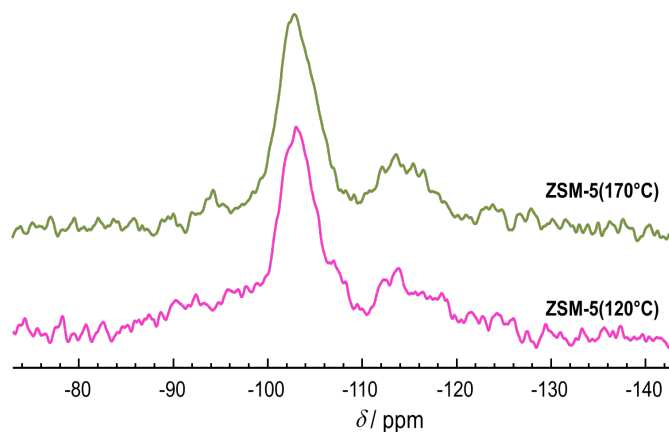
5 **Figure 6.** [29]Si {[1]H} cross-polarization spectra of nanosized zeolites prepared at 120 and 170 °C.

6

7 the method is the overlapping of Si(nAl) and Si(nOH) signals, consequently the calculated Si/Al

8 ratio value is usually lower than the actual one. Since the total sum of the intensities in the

9 normalized ^{29}Si {^{1}H} CP NMR spectra of the studied samples is practically equal it can be assumed

10 that the contribution of Si(3Si, 1OH) moieties to the broad signal at -103 ppm in ^{29}Si NMR spectra

11 is nearly identical in all of the samples. Hence the ^{29}Si NMR data can be used for calculation of

12 framework Si/Al. Obtained values are listed in Table 1 (column Si/Al[NMR]). They are higher than the

13 Si/Al ratio determined by chemical analysis. In the case of samples prepared at 120, 150 and 170 °C

14 the Si/Al ratio is very similar, approximately 36, while for ZSM-5(100°C) is 46. The different

15 values of Si/Al[NMR] when compared with bulk chemical analysis (Si/Al[ICP]) are attributed to the

16 presence of extra-framework Al species. This finding represents another indication on the presence

17 of amorphous material and extra-framework Al in the samples.

18 The nature of hydroxyl groups was studied by FTIR spectroscopy. In Figure 7 are displayed the

19 FTIR spectra of studied materials taken after their activation at 500 °C under high vacuum. The

20 studied range is between 3800-3000 cm^{-1} which corresponds to stretching vibrations of hydroxyl

21 groups. In this region five different features of the spectra can be observed. All samples exhibit a

22 broad low intensity band in the range 3550-3500 cm^{-1}. Generally this band is ascribed to silanol

23 nests that consist of a certain number of silanol groups interacting through hydrogen bonding. These

24 groups are usually situated at crystal steps or extended defects.[48,49] This corroborates the finding

25 from NMR where defects were detected as well. The low intensity of the band suggests relatively

26 limited amount of such sites.
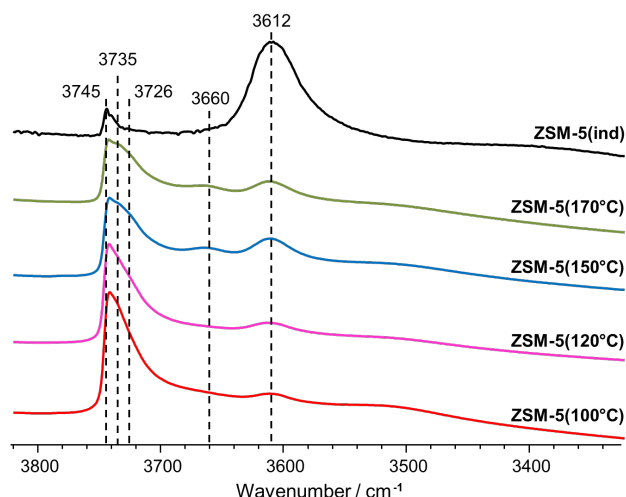
1 **Figure 7.** FTIR spectra in OH region of the industrial and nanosized zeolites synthesized at
2 different crystallization temperatures.

3

4 The band at 3612 cm^{-1} is related to Brønsted acid sites, more precisely hydroxyl groups bridging Si
5 and Al (Si–OH–Al).[48,49] The intensity of this band for nanosized ZSM-5 samples is significantly
6 lower than the reference ZSM-5(ind). The intensity of the band decreases with decrease of the
7 temperature of crystallization. On the other hand, the nanosized zeolites exhibit a more intense band
8 at about 3740 cm^{-1} in respect to the industrial sample. This band can be decomposed into three
9 peaks at 3745 cm^{-1}, 3735 cm^{-1} and 3726 cm^{-1}. They are assigned to isolated silanols at external
10 surface, weakly interacting internal silanols possibly near structural defects (intracrystalline Si–OH)
11 and internal silanols in zeolite channels, respectively.[48,50,51] The contribution of different peaks
12 varies in the set of nanosized samples. Thus, the peak at 3745 cm^{-1} is more intense for ZSM-
13 5(100°C) and ZSM-5(120°C) due to the larger external surface area. ZSM-5(150°C) and ZSM-
14 5(170°C) exhibit less intense and broader band owing to their lower external surface area and
15 therefore higher contribution of internal silanol groups. As already mentioned, the most expressed
16 feature in the spectra of ZSM-5(ind) corresponds to Brønsted acid sites (3612 cm^{-1}) with very small
17 impact of silanols. Such a marked difference between nanosized and microsized ZSM-5 samples
18 of comparable Si/Al ratio was already reported.[48,52,53] As mentioned, this feature of nanosized
19 zeolites is due to the large external surface area and large amount of defects. The results of FTIR
20 study are in line with the NMR data and confirm the large presence of hydroxyls in nanosized
21 materials.

22 In the spectra of samples ZSM-5(150°C) and ZSM-5(170°C) is observed a weak band in the range
23 3645-3680 cm^{-1} which is usually assigned to tetrahedral AlOH groups partially attached to the
24 framework.[25,26] In these two samples a barely observable peak at 3780 cm^{-1} usually associated with

11

1 octahedral extra-framework Al species was found.[54,55] These features do not exist in the spectrum

2 of the samples prepared at 100 and 120 °C. The result corroborates well with the assignments of

3 ^{27}Al MAS NMR resonances. Namely, besides the framework Al the ZSM-5(150°C) and ZSM-

4 5(170°C) samples exhibit highly distorted tetrahedral Al species not fully bound to the framework

5 (IR 3645-3680 cm^{-1}, ^{27}Al NMR 38 ppm) and octahedral extra-framework Al (IR 3780 cm^{-1}, ^{27}Al

6 NMR 4 and 0 ppm). The samples ZSM-5(100°C) and ZSM-5(120°C) include mostly crystalline

7 (^{27}Al NMR 53 ppm) and some amorphous material with five- (^{27}Al NMR 29 ppm) and six-fold

8 (^{27}Al NMR 7 ppm) coordination. It seems that amorphous aluminosilicate phase formed during low

9 temperature crystallization does not contain a lot of OH groups since only zeolite framework bands

10 were found in the corresponding IR spectra.[56]

11 The samples were further characterized by FTIR using pyridine as a probe molecule to discriminate

12 between Brønsted and Lewis acid sites. In Figure 8 are depicted normalized IR spectra of zeolite

13 samples with pyridine adsorbed at 150 °C. They were normalized with respect to the mass of the

14 self-supported disc of each sample. In the range of 1400-1700 cm^{-1}, chemically adsorbed pyridine

15 was revealed by the usual set of bands: two bands at 1545 and 1622 cm^{-1} assigned to pyridinium ion

16 (PyrH$^+$), two bands at 1454 and 1637 cm^{-1} related to coordinatively adsorbed pyridine and the

17 superposition of signals of the species adsorbed on Lewis and Brønsted sites at 1491 cm^{-1}. The
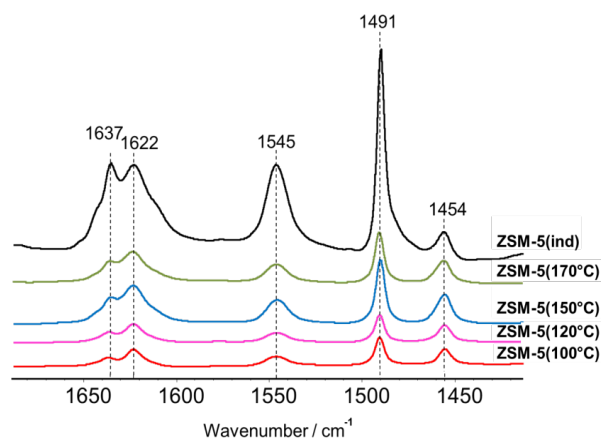
18 **Figure 8.** FTIR spectra after adsorption of Py over industrial and nanosized zeolites prepared at

19 different crystallization temperatures.

20

21 concentrations of Brønsted (B) to Lewis (L) acid sites calculated based on published extinction

22 coefficients for the bands at 1545 cm^{-1} and 1454 cm^{-1}, are given in the Table 2. The results suggest

23 that nanosized samples have at minimum 3 times lower amount of Brønsted acid sites in

24 comparison with industrial sample but similar amount of Lewis acid sites. The amount of Brønsted

25 acid sites decreases with decrease of the synthesis temperature. The highest number of Brønsted

acid sites (189 µmol/g) exhibits ZSM-5(150 °C) while this amount is two times lower for ZSM-5(100°C). This result correlates well with the results of ^{27}Al MAS NMR and OH-FTIR analyses. It is important to note that decrease of the amount of Brønsted acid sites is not accompanied by increase of Lewis acidity. It supports the previous assumption that the sample crystallized at low temperature contains some extra framework Al (EFAl), but this aluminum is namely present in low acidic form, most probably as dense amorphous aluminosilicate.

The strength of the acid sites was studied by pyridine desorption during increase of the temperature of the sample under continuous evacuation. Figure 9 shows that increase of the temperature leads to decrease of the intensity of the peaks of pyridine adsorbed over Brønsted and Lewis acid sites. Higher strength of the acid sites should result in the higher temperature necessary for desorption of pyridine. Adsorption of pyridine over Brønsted acid sites is stronger than over Lewis acid sites, however, at high temperatures there is a stable form of pyridine over Lewis acid sites which cannot be easily desorbed. Figure 9 indicates on the comparable strength of the Brønsted acid sites in the industrial sample and the samples crystallized at 150 and 170 °C. Samples crystallized at low temperatures (100 °C and 120 °C) demonstrate rather lower strength of the acid sites. Similar trend was observed in the case of Lewis acid sites, i.e., the acid strength decreased slightly with the decrease of the crystallization temperature. This result correlates well with observed lower

Table 2. Si/Al ratio and concentration of Brønsted (B) and Lewis (L) acid sites determined by IR analysis of adsorbed pyridine (Py).

Sample	Si/Al^{ICP}	n(B-Py) µmol g^{-1}	n(L-Py) µmol g^{-1}
ZSM-5(ind)	25	582	128
ZSM-5(170°C)	27	138	126
ZSM-5(150°C)	31	189	155
ZSM-5(120°C)	25	89	114
ZSM-5(100°C)	35	79	88

crystallinity of the samples synthesized at lower temperature. Comparable effect was reported during the dealumination[57] or recrystallization of zeolites[58]. It is in line with the theory that stronger sites are located in the areas with high crystallinity and long range symmetry, while weak sites exist in non well-crystallized areas.[59]
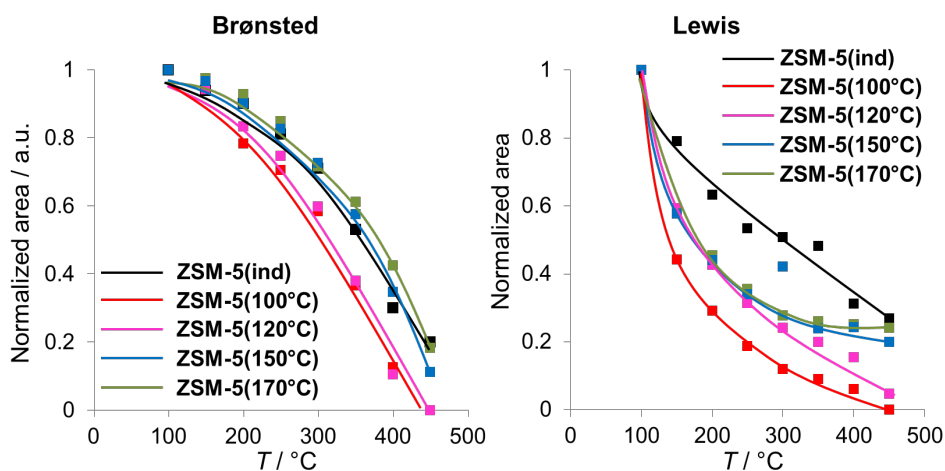
Figure 9. Normalized area for adsorbed Py over Brønsted (1545 cm^{-1}) and Lewis (1454 cm^{-1}) acid sites during desorption with increase of the temperature over industrial and nanosized zeolites prepared at different crystallization temperatures.

Catalytic performance and catalysts deactivation

Figure 10 shows the methanol conversion over homemade and industrial catalysts as a function of TOS at 450 °C. Initially, all the catalysts show near 100 % conversion. The rate of deactivation differs substantially than the industrial sample, which lost activity after 30 h on stream. The conversion profiles of other catalysts widely varied with the crystallization temperature: ZSM-5(120°C) and ZSM-5(170°C) deactivated after 60 h of test, while ZSM-5(150°C) demonstrated higher stability and was active up to 80 h. The best performance was recorded for ZSM-5(100°C) sample which deactivated after 100 h of the reaction.

The major products of the MTO reaction over all samples were light alkanes and olefins such as ethylene, propylene, and butenes (Table 3, Figure 11) with the selectivity to these products about 60 % at 20 h TOS (Table 3). Heavier hydrocarbons and aromatics (C_5^+) contribute to the rest of the products. ZSM-5(ind) catalyst demonstrated significant selectivity to light alkanes at the beginning of the test. Figure 11 shows that the yield of light alkanes is decreasing and the production of light olefins is increasing in time over ZSM-5(ind). Thus, the yield to propane is decreasing from 22 to 2 % while the yield to propylene increases from 4 to 29 % during the first 35 h of the test. It is interesting to note that although the ratio of olefins to alkanes changes significantly during the reaction the ratio of propylene to ethylene is not much affected. The ratio C_3H_6/C_2H_4 increases from

14
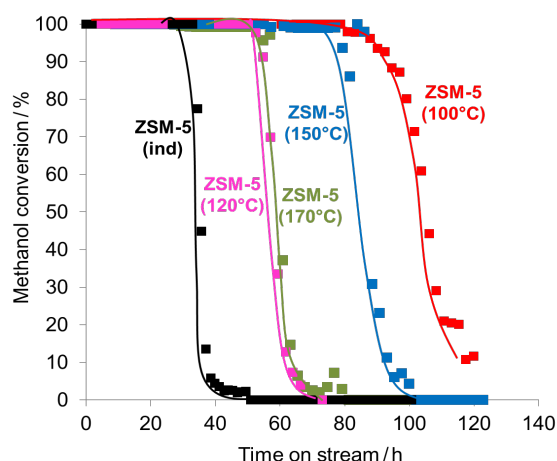
Figure 10. Methanol conversion versus time on stream over industrial and nanosized zeolites prepared at different crystallization temperatures (T= 450 °C, p=0.1 MPa, WHSV=1 h^{-1}).

1 to 1.3 which is close to the ratio usually observed over ZSM-5 catalysts (Table 3). Light alkanes and aromatics are referred to as hydrogen transfer products in the MTO reaction. The hydrogen transfer activity is usually measured in methanol chemistry by Hydrogen Transfer Index (HTI), which is defined as the ratio of C_4 alkanes to the total C_4 concentration (C_4 alkanes and olefins). High HTI indicates a high activity in transformation of olefins to aromatics and alkanes. ZSM-5(ind) shows HTI 0.65 at 20 h TOS (Table 3).

MTO reaction over nanosized zeolites shows significantly different behavior in comparison with the industrial sample. Nanosized samples show much higher selectivity to light olefins with lower contribution of heavier hydrocarbons (C_5^+), aromatics and C_1-C_4 alkanes (Table 3). Thus, ZSM-5(170°C) has almost two times lower selectivity (12.4 %) to light alkanes and almost two times higher selectivity to light olefins (54.6 % for ZSM-5(170°C) in respect with ZSM-5(ind)). In

Table 3. MTO reaction over studied ZSM-5 catalysts (T= 450°C, p=0.1 MPa, WHSV=1 h^{-1}, TOS = 20 h).

| Sample	Conv. (%)	Selectivity (C- mol %)					C_3H_6/C_2H_4	HTI-C_4
		C_1-C_4	C_2H_4	C_3H_6	C_4H_8	C_5^+		
ZSM-5(ind)	100	25.0	14.6	14.9	3.1	42.4	1.0	0.65
ZSM-5(170°C)	100	12.4	22.3	26.6	5.7	33.0	1.2	0.43
ZSM-5(150°C)	99.5	10.1	17.5	24.2	5.3	42.9	1.4	0.42
ZSM-5(120°C)	99.7	8.0	11.3	42.0	10.4	28.3	3.7	0.33
ZSM-5(100°C)	99.9	7.7	8.4	53.3	14.3	16.3	6.3	0.30
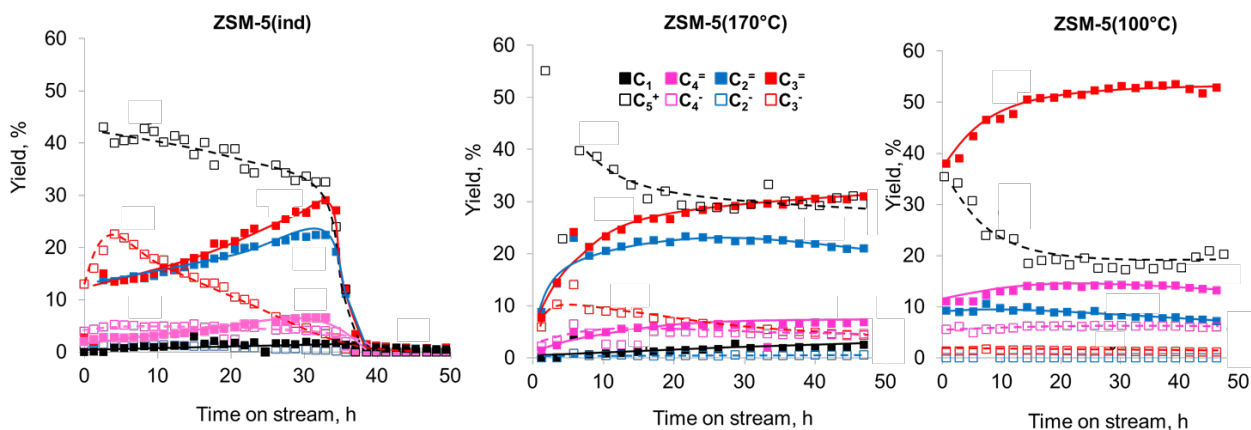
Figure 11. Products yield during MTO reaction over ZSM-5(ind), ZSM-5(170°C) and ZSM-5(100°C) versus time on stream (T= 450°C, p=0.1 MPa, WHSV=1 h^{-1}).

contrast with the industrial material the sample synthesized at ZSM-5(170°C) does not show abrupt changes in the distribution of the hydrocarbons with time on stream and the selectivity to propylene is moderately increasing in time. On the other hand, the selectivity to ethylene is slightly decreasing. Nanosized sample demonstrates significantly lower hydrogen transfer activity in comparison with ZSM-5(ind). Indeed, HTI decreases from 0.65 for ZSM-5(ind) to 0.43 for ZSM-5(170°C). It explains lower selectivity to alkanes and aromatics and higher selectivity to light olefins. Note that despite of significant changes in the products distribution the ratio of propylene to ethylene for nanosized sample ZSM-5(170°C) remains similar to the industrial sample (Table 3). Further, for the sample prepared at 150 °C the ratio of propylene to ethylene is similar to ZSM-5(170°C), 1.4. Interestingly, this sample showed similar HTI but lower selectivity to olefins in comparison with ZSM-5(170°C) – 47 and 54.6 %. Significant change in P/E ratio is observed for the ZSM-5(120°C) and ZSM-5(100°C), 3.7 and 6.3 respectively. Moreover, the decrease of the temperature of crystallization results in further decrease of the hydrogen transfer activity – from HTI of 0.42 (150 °C sample) to 0.3 (100 °C sample) and selectivity to light alkanes and C_5^+ hydrocarbons. These changes are coupled with increase of the selectivity to olefins – at 20 h TOS the selectivity to propylene is 42.0 % over ZSM-5(120°C) and 53.3 % over ZSM-5(100°C) catalyst.

In Figure 12 is displayed the correlation of the ratio of propylene to ethylene with the reciprocal HTI. It shows that lower HTI results in higher selectivity to propylene. The effect of HTI on the selectivity is not linear and increases significantly at low values of hydrogen transfer activity.
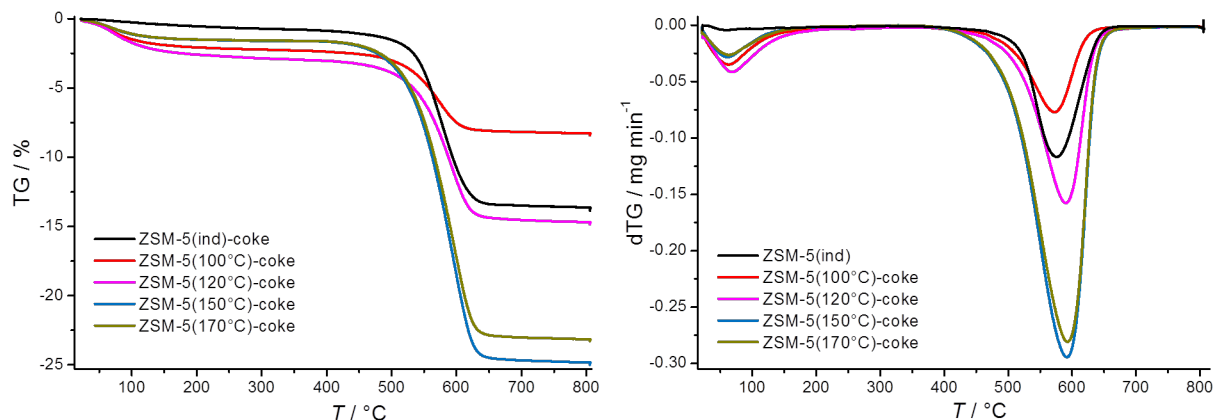
TG analysis of the spent nanosized ZSM-5 samples (after 120 h TOS) was performed. The TG curves exhibit first weight loss in the range from room temperature till 140 °C which is attributed to desorption of volatile species (Figure 13). The weight content of these species is from 1.4 wt % for the sample ZSM-5(170°C) to 2.4 wt % for ZSM-5(120°C). The industrial sample does not show any
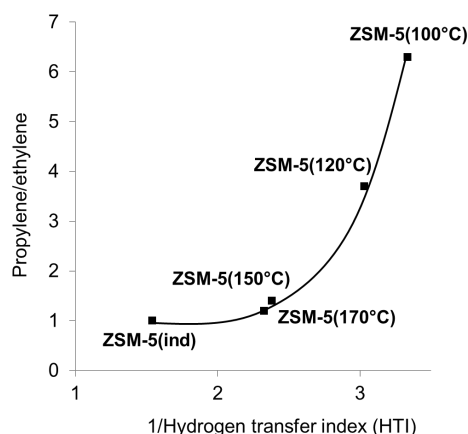
Figure 12. Propylene to ethylene ratio versus reciprocal HTI over industrial and nanosized zeolites prepared at different crystallization temperatures (T= 450°C, p = 0.1 MPa, WHSV = 1 h^{-1}, TOS = 20 h).

significant changes in this temperature range revealing that there are almost no physisorbed species in this sample. The second weight loss, in the range 430 - 650 °C, is attributed to highly condensed polyaromatic residues, often denoted as high-temperature coke. The sample ZSM-5(100°C) contains markedly lower amount of the coke than other studied samples (6.34 %). The industrial sample and the sample prepared at 120 °C comprise similar quantity of carbonaceous deposits, 12.64 and 12.26 % respectively. In the samples synthesized at high temperature there is almost three times higher amount of coke than in 100 °C sample – 23.39 % in ZSM-5(150°C) and 21.71 % in ZSM-5(170°C). The position of minimum of dTG curve (Table 3, Figure 13) of the sample ZSM-5(100°C) and ZSM-5(ind) is at approximately identical temperature – 572 and 575 °C, respectively. On the other hand, the minimum in other samples is found at 590 and 593 °C. Furthermore, the range where the change takes place is notably broader for the samples prepared at higher temperature, 150 and 170 °C. The obtained results clearly indicate difference in the nature, stability and location of the coke species deposited on the studied catalysts (Table 4).

Figure 13. TGA (left-hand side) and dTG (right-hand side) curves of the studied nanosized and industrial ZSM-5 catalysts after being used in the MTO reaction.

Table 4. The TG and nitrogen adsorption analysis of the spent nanosized and industrial ZSM-5 catalysts in the MTO reaction. Weight loss and the dTG minimum are given for the range from 430 to 650 °C.

Sample	weight loss %	T_{min} °C	S_{BET} m^2g^{-1}	V_{mic} cm^3g^{-1}	S_{ext} m^2g^{-1}	V_{total} cm^3g^{-1}
ZSM-5(ind)	12.64	575	41	0.02	2	0.200
ZSM-5(170°C)	21.71	593	188	0.07	25	0.254
ZSM-5(150°C)	23.39	593	181	0.07	27	0.264
ZSM-5(120°C)	12.26	590	273	0.11	57	0.411
ZSM-5(100°C)	6.34	572	359	0.12	77	0.488

Nitrogen adsorption measurements of spent catalysts show different degree of pore blockage. (Table 4). The micropore volume of the industrial samples is fully blocked by coke species, while the decrease of micropore volume varies between 60 and 15 % for the nanosized ZSM-5 samples. More precisely, 60 % decrease of the micropore volume is observed for ZSM-5(150°C) and ZSM-5(170°C) samples. The decrease for ZSM-5(120°C) and ZSM-5(100°C) is 25 and 15 %, respectively. These data match well with the TGA results which showed higher coke content in the samples synthesized at 150 and 170 °C. ZSM-5(120°C) and ZSM-5(ind) exhibit similar amount of coke. Nevertheless, the micropore volume of nanosized sample remains partially accessible for the N_2 molecule, while the micropore volume of micron-sized crystals is fully blocked (Table 4). The most plausible explanation of this phenomenon is the shorter diffusion path in the nanosized sample, which allows substantial part of the coke to migrate and deposit on the external surface of the crystallites. This statement is based on a previous study which showed that the coke species are

1 deposited on the external surface of nanosized ZSM-5 crystals, in contrast to the abundant coke

2 formation in the pores of the micron-sized counterpart.[60] Different nature of the coke formed in the

3 nano- and micron-sized crystals could also contribute to the observed differences in the accessibility

4 at similar coke content.
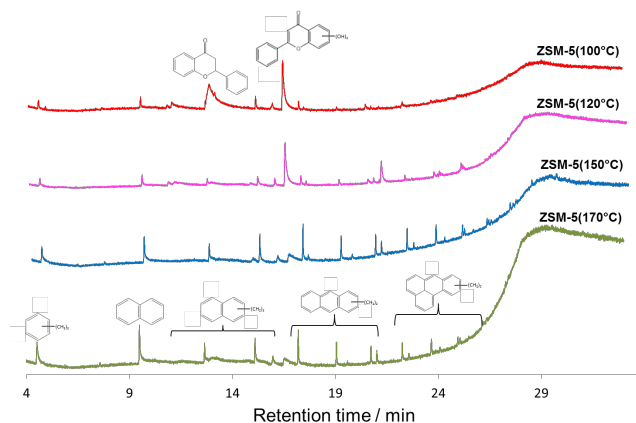
5 **Figure 14.** GC-MS analyses of organics extracted by dichlormethane from the spent nanosized

6 ZSM-5 catalysts.

7 In order to ascertain the nature of the coke species in the spent ZSM-5 catalysts, the samples were

8 treated with toluene. Any organic compound was found in the extracted solvent showing the

9 absence of dissolvable coke in the spent catalysts. Further, the zeolite has been dissolved in HF and

10 the organic part extracted with dichlormethane. The coke molecules were subjected to GC-MS

11 analysis (Figure 14). The GC-MS analysis of the coke formed in the ZSM-5(ind) did not provide

12 peaks that could be used to reveal the nature of the coke. Obviously, mostly "heavy" coke insoluble

13 in toluene and CH_2Cl_2 was formed in the industrial sample. The chromatograms of the samples

14 ZSM-5(150°C) and ZSM-5(170°C) are almost identical and show presence of alkylated polycyclic

15 aromatic compounds like naphthalene and anthracene. It is important to note that there is larger

16 variety of coke species in the samples ZSM-5(150°C) and ZSM-5(170°C) which contain the highest

17 amount of coke. Only traces of polycyclic aromatic compounds were found in the ZSM-5(100°C)

18 and ZSM-5(120°C). New partially hydrogenated oxygen containing species on the basis of oxane

19 have been observed in the chromatograms. The coke analysis of ZSM-5(100°C) differs substantially

20 in the elemental composition and in the region of heavier species where a negligible amount of coke

21 was found. The 120 °C sample is a merger between ZSM-5(100 °C) and ZSM-5(150°C)/ZSM-

22 5(170°C). There are peaks corresponding to heavier species present in its chromatogram together

23 with peaks found in ZSM-5(100 °C), but of significantly lower intensity. Likewise, as the coke

24 quantity decreases it becomes less diverse (complex) leading to the conclusion that the factors

25 causing the deactivation of the catalysts differ in the studied set of the samples.

26 The analysis of the spent ZSM-5 catalysts shows that the insoluble coke in the industrial sample

19

comprises highly polyaromatic species of graphitic character. Although the amount of coke is lower than in the case of ZSM-5(150°C) and ZSM-5(170°C) samples, the micropore volume is completely blocked. It can be assumed that the coke is namely situated in the intersections of straight and zig-zag channels, thus blocking the access to active sites. On the other hand, the nanosized sample retain certain degree of microporosity, even in the case of ZSM-5(150°C) and ZSM-5(170°C) samples, which exhibit almost two times higher coke content. This result unambiguously proves that a substantial part of the coke is deposited on the external surface of zeolite nanoparticles and a certain part of micropore volume remains accessible.

Discussion

The catalytic performance of the industrial ZSM-5 sample in the MTO reaction is similar to the results reported in the literature.[13,14] We have employed this sample as a reference in order to evaluate the catalytic performance to the nanosized ZSM-5 synthesized under different temperature and thus to apprehend better the impact of physiochemical properties on zeolite activity. Namely, the differences with respect to the size and acid site density provide broader range of the studied factors and subsequently the overall process can be elucidated to a greater degree as it is going to be demonstrated in the forthcoming discussion.

The dual cycle mechanism is generally accepted for methanol to olefins formation over ZSM-5. Basically, ethylene and equal quantity of propylene are generated by the aromatic based hydrocarbon pool mechanism (aromatic cycle), while higher olefins are generated by olefins methylation and subsequent cracking (alkene cycle).[18] Hydrogen transfer reaction is a secondary reaction in MTO process and represents a connection between the two cycles. It involves the transformation of higher alkenes formed in the alkene cycle to alkanes and aromatics. Brønsted acid sites are required for the methanol dehydration[61] and to promote the formation of the hydrocarbon pool species. In addition, polycyclic aromatic species formed on Brønsted acid sites enhance the probability of catalysts deactivation. On the contrary, the alkene pathway is promoted by low catalyst acidity. It is important to note that the catalyst activity and deactivation can be affected by different factors. For example, the catalytic activity depends on the diffusion rate of the methanol or DME while deactivation is a function of the diffusion of hydrocarbon species, expectedly polymethylbenzenes in the case of ZSM-5 catalyst. As already mentioned, the crystal size and textural properties have also been shown to play an important role in the MTO catalyst performance.[18]

The distinct product selectivities, propylene to ethylene ratio and HTI clearly indicate the differences in the mechanism of the MTO reaction over the studied set of samples. There are two

extreme examples – the sample ZSM-5(100°C) and ZSM-5(ind). In the industrial sample the propylene/ethylene ratio is the lowest and HTI the highest at 20 h TOS (Figure 12, Table 3). Large crystals and high acid site density in the ZSM-5(ind) favor ethylene formation. ZSM-5(170°C) exhibits similar propylene to ethylene ratio (1.2), but higher selectivity towards both ethylene and propylene. Moreover, HTI is lower for the ZSM-5(170°C) sample. Although these two catalysts demonstrate similar propylene/ethylene ratio (Table 3), the different selectivities should arise from lower amount of acid sites and the smaller crystal size of the later catalyst. The situation is opposite for the ZSM-5(100°C) and ZSM-5(120°C) samples which exhibit slightly smaller size in respect to ZSM-5(170°C) yet substantially lower acidity. The propylene is the major product of the reaction for these two samples. Different carbon species formed on different zeolites provide another strong indication of different predominant reaction pathways over these samples. The nature of the coke formed on different samples also suggests different reaction mechanism. Indeed, the samples crystallized at lower temperatures (100°C and 120°C) contain totally different types of coke species in comparison with zeolites obtained at higher temperatures (150°C and 170°C). Predominant non-aromatic coke species formed on ZSM-5(100°C) and ZSM-5(120°C) point out that the alkene cycle controls the reaction leading to selective propylene synthesis. The main difference between the samples synthesized at low and high temperatures is the acid sites strength and the external surface area (Table 1). The observed variation in catalytic performance and the selectivity in particular is a consequence of the impact of different factors. Figure S1 shows the dependence of C3 yield versus number of Brønsted acid sites defined by Py adsorption. For example, catalysts crystallized at 100 ºC, 120 ºC and 150 ºC have very similar amount of acid sites according to solid state NMR and FTIR adsorption of Py, however, the yield of propylene is much lower in the case of ZSM-5(100°C). Thus, the acid sites density seems to have a negligible effect on the propylene selectivity. At the same time, there is a clear dependence of propylene yield on the relative strength of acid sites defined by pyridine desorption at 200 ºC (Figure 9). The yield of propylene (Figure S2, SI) clearly increases with decrease of the strength of acid sites which indicates the key role of this factor in the reaction. We attribute lower acidity of 100 °C and 120 °C samples to more defected structure of zeolites synthesized under milder conditions. These samples exhibit also higher external surface and larger presence of surface silanols (Figure 7).

Another possible explanation of significant change in the catalytic behavior of the catalysts synthesized at low temperature could be the presence of extra-framework Al and defected silanols groups. These sites might possess weak acidity and participate in activation of methanol to olefins. In order to check this assumption we have synthesized aluminum-rich sample using TPAOH as a structure directing agent. In order to maximise the amount of extra-framework Al species and surface hydroxyls we have employed a gel with Si/Al ratio of 5, which is much lower that a TPA

templated ZSM-5 can accommodate in the framework. The resultant material is X-ray amorphous (Figure S3, SI) containing micropores (Figure S4, SI) and tetrahedral (framework) and octahedral (extra-framework) aluminium according to ^{27}Al MAS NMR (Figure S5, SI) without ZSM-5. Adsorption of Py revealed the presence of significant amount of Lewis acid sites formed by extra-framework aluminium and much lower amount of Brønsted acid sites formed by tetrahedral aluminium (Table S1, SI). Further, in this material the isolated silanols at external and internal surface are by far the most dominant type of OH groups (Figure S6, SI). Catalytic test of this material conducted at the same reaction conditions as in the case of nanosized and industrial ZSM-5 samples did not show any activity in methanol transformation to olefins. We attribute this result to the fact that the Brønsted acid sites in amorphous material have too low strength as shown by desorption of Py at 300 °C (Table S1, SI). These data show that neither extra-framework aluminium nor silanol groups cannot be responsible for methanol transformation to propylene over studied set of nanosized ZSM-5 samples. The results show also that the catalyst for this reaction cannot be totally amorphous. Herein, shorter diffusion path and larger surface for deposition of aromatic species in these samples propagate propylene formation as previously reported in literature.[62]

The lifetime of the industrial sample is three times shorter than ZSM-5(100°C) and two times shorter than ZSM-5(170°C) revealing the negative effect of higher acid site density and larger crystal size on the MTO reaction. This finding is in line with the studies where at high reaction temperature and acid site density large graphite-like coke compounds are formed in large ZSM-5 crystals inducing pore blocking.[63] In summary, the coke rate formation is enhanced with the increasing acidity of the material, while the large crystal size limit the coke migration to the external surface of the crystals and thus the pores are rapidly blocked. Here might be the reason for the observed increase of the propylene and ethylene yield during the first 35 h of the test (Figure 11). It was shown previously that the quantity of the aromatics increases with the time on stream.[63] Aromatic species are not only coke precursors, they are indispensable for the aromatic cycle that may result in: 1) increased amount of ethylene and propylene generated by aromatic cycle; and 2) continuous poisoning of the Brønsted acid sites. Consequently, the selectivity towards ethylene and propylene should be rising as long as the diffusion through the crystal is possible. The longest catalyst lifetime of the ZSM-5(100°C) sample can be explained in terms of lower acid site density, somewhat lower acid strength, shorter diffusion path and larger external surface area. The moderate acidity of ZSM-5(100°C) is particularly appropriate for the MTO reaction, while the lower acid site density together with short diffusion path hinder the pore blocking. Thus the catalyst lifetime is extended even upon partial blocking of the active sites.[64]

ZSM-5(120°C), ZSM-5(150°C) and ZSM-5(170°C) exhibit catalytic behavior in between the sample prepared at 100 °C and the industrial sample. Decrease of the propylene/ethylene ratio and

selectivity towards propylene with rising the ZSM-5 synthesis temperature can be attributed to variations in the contributions of MTO reaction pathways from primary alkene towards primary aromatic cycle due to the higher acidity, lower external surface area and slight, but still notable increase of the crystal size. TG and nitrogen adsorption data imply that more and more coke is generated as the crystallization temperature gets higher and crystals get larger. The only surprising feature is the unexpectedly short catalyst lifetime of the 120 °C sample, 60 h. In term of physicochemical properties this sample is situated between ZSM-5(100°C) and the samples synthesized at higher (150 and 170°C) temperatures. There is not a particular feature of this sample that we could relate with shorter lifetime. On the other hand, ZSM-5(120°C) stays between ZSM-5(100°C) and high temperature samples in term of propylene selectivity.

Hydrogen transfer reaction rates depend on the amount of acid sites, strength and the structure of zeolite.[65,66] It has been shown that on Al_2O_3 adjacent acid sites rapidly participate in hydrogen transfer.[67] Hence, in the case of ZSM-5(ind) the presence of high amount of strong acid sites leads to intensive hydrogen transfer reaction with formation of alkanes and condensed aromatic structures resulting in coke deposition and total pore blocking. As expected, the HTI value is getting lower with the decreasing acid site density. However, the lower amount of acid sites and larger crystal sizes in ZSM-5(170°C) does not lead to significant changes in propylene/ethylene ratio. At the same time, the decrease of the acid sites density and strength of acid sites in the nanosized zeolites having slightly lower size of the crystals but different external surface area leads to further decrease of hydrogen transfer activity. Indeed, the plot of HTI versus number of Brønsted acid sites (Figure S7, SI) does not show clear correlation which points out the importance of acid site strength in hydrogen transfer. The obtained data suggest that the mechanism of the MTO reaction is a result of complex interplay between particle size, number and strength of active sites.

To sum up, the best catalytic performance has been attained over zeolite crystallized at the lowest temperature (100 °C). The catalyst demonstrated the highest stability and selectivity to propylene. The propylene and light olefins yield over ZSM-5(100°C) is compared with the available literature data (Table S2). As can be seen the catalyst obtained at very low temperature demonstrates the highest selectivity to propylene and yield of light olefins. The ratio of propylene to ethylene was 6.3 and the selectivity to propylene 53 %, which is among the highest selectivities reported in the literature .[10-17, SI 1-7] The most important characteristics of this catalyst are very small nanosized particles built of intergrown crystalline domains responsible for large external surface area and their lower acid sites strength and density.

Conclusions

The impact of crystallization temperature on the physicochemical properties of ZSM-5 is investigated. The lowering of the crystallization temperature from 170 °C to 100 °C resulted in decreasing the size of crystalline domains, slight decreasing of the particle size from 140 to 100 nm, rising of the external surface area, lower crystallinity and reduced acid site density and strength. The crystallization at lower temperatures (100 and 120 °C) led to reduced incorporation of aluminium in the zeolite framework and deposition of amorphous alumosilicate species within the ZSM-5 particles.

Nanosized zeolites exhibit much higher stability in comparison with the industrial micron-sized sample of similar bulk Si/Al ratio. In addition, the overall selectivity to olefins and especially to propylene is getting higher as the zeolite preparation temperature is decreasing. The set of experimental data revealed that this effect is due to the shift from prevailing aromatic-based to olefin-based cycle in MTO reaction. Namely it has been shown that these two simultaneously occurring cycles can be adjusted by varying the acid site density, acid sites strength, the size of zeolite crystals and the external surface area. Consequently, the selectivity towards desired product can be obtained. Herein was realized the highest selectivity to propylene of 53 % with propylene to ethylene ratio 6.3 over nanosized ZSM-5 catalyst crystallized at 100 °C. Thus, the zeolite synthesis conditions and the crystallization temperature in particular could be used to tune the catalytic activity of zeolites.

Experimental Section

Catalyst preparation

The first step in the preparation of the nanosized ZSM-5 crystals was mixing of the appropriate amounts of sodium aluminate (NaAlO$_2$, Riedel de Haën, w(Al$_2$O$_3$) = 54 %, w(Na$_2$O) = 41 %), tetrapropylammonium hydroxide (TPAOH, Alfa Aesar, 20 wt. % water solution) and distilled water. The mixture was agitated with magnetic stirrer until the system became clear. Thereafter, tetraethoxysilane (TEOS, Aldrich, 98 %) was added to the solution and hydrolyzed at 80 °C for 24 h. The final molar oxide composition of the reaction mixture was 1.23Na$_2$O:9.74TPAOH:1.0Al$_2$O$_3$:43.2SiO$_2$:806H$_2$O. Aliquots of clear solution were divided in four autoclaves and heated at 100, 120, 150 and 170 °C. The synthesis at 100 °C was performed for 7 days. The duration of the syntheses at 120, 150 and 170 °C was 5 days. The prepared samples are further referred as ZSM-5(100°C), ZSM-5(120°C), ZSM-5(150°C) and ZSM-5(170°C). Recovered solid phases were washed with distilled water until the pH of the supernatant was 7, dried at 80 °C and calcined at 550 °C for 5 h (heating rate 1.75 °C/min). The calcined zeolites were three times ion

exchanged with ammonium chloride solution ($c(NH_4Cl)$ = 0.5 mol/dm^3) at 80 °C. For the sake of comparison, commercial zeolite ZSM-5 (NH$_4$-form), denoted here as ZSM-5(ind), offered by Süd-Chemie (Clariant), lot number BEEZ 01081, was used in this study. The protonic forms were obtained by calcining the NH$_4$-form of zeolites at 550 °C for 5 h with the heating ramp of 1.75 °C/min in static air.

The amorphous material was synthesized using tetrapropylammonium hydroxide (TPAOH, Alfa Aesar, 1M), tetraethoxysilane (TEOS, Aldrich, 98%), di-sec-butoxyaluminoxytriethoxysilane (DSBATES, ABCR GMBH) and doubly distilled water. The needed amount of TPAOH was mixed with the water in a polypropylene bottle. Then DSBATES was added and the mixture was stirred for 24 h followed by the addition of TEOS. The solution was stirred for additional 24 h and subsequently treated for 10 days at 100 °C in an oven. The molar composition of the reaction mixture was 25 DSBATES : 9 TPAOH : 125 TEOS : 500 H$_2$O. The recovered solid phase has been washed three times with acetone and then with water until neutral pH. The calcination was performed at 550°C for 5 h.

Physicochemical characterization

The phase composition of the solid samples was analyzed by X-ray diffraction using PANalytical X'pert PRO MPD diffractometer with CuK$_\alpha$ monochromatized radiation (λ = 1.5418 Å, 45 kV, 40 mA). The measurements were performed in the range of Bragg's angles 2θ = 5-50 °, step size of 0.0167 °, time per step of 99.68 s.

The electron micrographs of the prepared crystals were obtained by MIRA-LMH (Tescan) scanning electron microscope (SEM) equipped with field emission gun. The elemental analysis of the studied ZSM-5 materials was performed by inductively coupled plasma–atomic emission spectrometer (ICP-AES) OPTIMA 4300 DV (PerkinElmer).

Solid state NMR spectra were recorded on a Bruker Avance III (11.7 T) spectrometer using 4 mm-OD zirconia rotors and a spinning frequency of 14 kHz. For ^{27}Al MAS NMR spectra pulse recycling delay was 1 s and a pulse length of 2.5 microseconds (π/12, selective pulse) was applied. Single pulse excitation (30 ° flip angle) of 3 μs was used for ^{29}Si MAS NMR experiment and 30 s of recycle delay. ^{29}Si {^{1}H} cross-polarization (CP) MAS experiments were performed with a contact time of 4 ms and a recycling time of 1 s. The chemical shifts were referenced to a 0.1 M aqueous solution of aluminium nitrate ($c(Al(NO_3)_3)$ = 0.1 mol/dm^3) and tetramethylsilane (TMS), respectively. The acquired spectra were normalized with respect to the weight of the corresponding sample.

Nitrogen adsorption/desorption of the calcined samples and the samples used in catalytic tests was performed with a Micromeritics ASAP 2020 automated gas adsorption analyzer. The samples were outgassed at 300 °C under a vacuum overnight prior to the measurement. Specific surface areas were determined from the BET equation. The total pore volume was taken from nitrogen adsorbed volume at $p/p_0 = 0.99$. The t-plot method was used to distinguish the micropores from the mesopores and to calculate the external surface area. The mesopore size distributions of solids were estimated by Barret−Joyner−Halenda (BJH) method.

FTIR measurements were carried out on a Nicolet Magna 550-FTIR spectrometer at 4 cm^{-1} optical resolution. The pressing of the samples into self-supported discs (diameter 2 cm, 13 mg) preceded the measurements. Before acquiring the spectra at room temperature, each sample was pretreated in the IR cell connected to the vacuum line at 20 °C (0.33 °C/min) for 1.5 h and at 500 °C (1.27 °C/min) for 2 h under pressure 10^{-6} Torr. The obtained spectra were normalized to the weight of the self-supported disc.

The adsorption of pyridine was performed at temperature of 150 °C. After establishing a pressure of 1 Torr at equilibrium, the cell was evacuated at room temperature. In order to study the strength of the interactions between the zeolite and the probe molecules, the samples were heated to 50-400 °C (step 50 °C) and the spectra were taken at each temperature. Then, the amount of Brønsted and Lewis acid sites at each desorption temperature was calculated from the integrated area of the bands (after background subtraction) of adsorbed pyridine at 1545 cm^{-1} and 1455 cm^{-1} using the extinction coefficients reported in literature.[67,68]

Thermogravimetric analysis (TG) of the samples after being used in the catalytic tests has been performed by employing Setaram Setsys TGA instrument. The samples were heated up to 800 °C with a rate of 5 °C min^{-1} in air flow.

Catalytic test

The samples were pressed into wafers and subsequently crushed and sieved to obtain particles in the range 100–200 μm. Each catalytic test was performed with 50 mg of catalyst in a fixed bed reactor configuration, with 2.0 mm inner diameter. Methanol has been added by saturation of 20 ml/min of N_2 by 0.075 ml/h of methanol, thus giving a WHSV (weight hourly space velocity) of 1.2 g methanol/g$_{zeolite}$/h. The product stream was analyzed with an Agilent gas chromatograph equipped with FID detector and automatic sampling (CP-Sil5 column). The catalyst temperature was adjusted to 450 °C before onset of methanol for all tests, and once the reaction had started the oven temperature was not further changed. Product selectivity was defined as the mole ratio of each product (on C_1 basis) referred to the moles of converted methanol. The following products were detected during the reaction: methane, CO, CO_2, light olefins and alkanes C_2-C_4 and higher

hydrocarbons. The column has been calibrated with identification of response factors of the methanol and main products of the reaction.

Coke analysis

The qualitative analysis of the soluble part of the coke was performed through GC-MS experiment (Shimadzu GCMS-QP2010S). Prior to the analysis the spent catalysts were treated with toluene. The remained powder was dissolved in 40 % HF with subsequent extraction of organic phase by dichloromethane.

References

[1]   C. D. Chang, *Catal. Rev. Sci. Eng.* **1983**, *25*, 1-118.

[2]   J. Q. Chen, A. Bozzano, B. Glover, T. Fuglerud, S. Kvisle, *Catal. Today* **2005**, *106*, 103-107.

[3]   H. Koempel, W. Liebner, *Stud. Surf. Sci. Catal.* **2007**, *167*, 261-267.

[4]   J. Cobb, New Zealand Synfuel: The story of the world's first natural gas to gasoline plant, vol. 1, Cobb/Horwood Publications, Auckland, New Zealand, **1995**.

[5]   B. P. C. Hereijgers, F. Bleken, M. H. Nilsen, S. Svelle, K. P. Lillerud, M. Bjorgen, B. M. Weckhuysen, U. Olsbye, *J. Catal.* **2009**, *264*, 77-87.

[6]   D. Chen, K. Moljord, A. Holmen, *Microporous Mesoposorus Mater.* **2012**, *164*, 239-250.

[7]   M. Bjorgen, F. Joensen, M. Spansberger Holm, U. Olsbye, K. P. Lillerud, S. Svelle, *Appl. Catal. A* **2008**, *345*, 43-50.

[8]   S. Zhang, B. Zhang, Z. Gao, Y. Han, *Ind. Eng. Chem. Res.* **2010**, *49*, 2103-2106.

[9]   Y. Jin, S. Asaoka, S. Zhang, P. Li, S. Zhao, *Fuel Process. Techn.* **2013**, *115*, 34 - 41.

[10] C. D. Chang, C. T.-W. Chu, R. F. Socha, *J. Catal.* **1984**, *86*, 289-296.

[11] D. Prinz, L. Riekert, *Appl. Catal.* **1988**, *37*, 139-154.

[12] M. Sugimoto, H. Katsuno, K. Takatsu, N. Kawata, *Zeolites* **1987**, *7,* 503-507.

[13] C. Mei, P. Wen, Z. Liu, H. Liu, Y. Wang, W. Yang, Z. Xie, W. Hua, Z. Gao, *J. Catal.* **2008**, *258*, 243-249.

[14] F. L. Bleken, S. Chavan, U. Olsbye, M. Boltz, F. Ocampo, B. Louis, *Appl. Catal. A* **2012**, *447-448*, 178-185.

[15] J. Liu, C. X. Zhang, Z. H. Shen, W. Hua, Y. Tang, W. Shen, Y. H. Yue, H. L. Xu, *Catal. Commun.* **2009**, *10*, 1506-1509.

[16] T. S. Zhao, T. Takemoto, N. Tsubaki, *Catal. Commun.* **2006**, *7*, 647-650.

[17] T. Taniguchi, K. Yoneta, S. Nakaoka, Y.Nakasaka, T. Yokoi, T. Tago, T. Masuda, *Catal. Lett.* **2016** *146*, 442-451.

[18] U. Olsbye, S. Svelle, K. P. Lillerud, Z. H. Wei, Y. Y. Chen, J. F. Li, J. G. Wang, W. B. Fan, *Chem. Soc. Rev.* **2015**, *44*, 7155-7176.

[19] M. Choi, K. Na, J. Kim, Y. Sakamoto, O. Terasaki, R. Ryoo, *Nature* **2009**, *461*, 246-249.

[20] A. A. Rownaghi, J. Hedlund, *Ind. Eng. Chem. Res.* **2011**, *50*, 11872-11878.

[21] W. Zhijian, W. Wu, G. Li, C. Wang, H. Yang, D. Zhang, *Appl. Catal. A* **2016**, *523*, 312-320.

[22] V. Valtchev, L. Tosheva, *Chem. Rev.* **2013,** *113*, 6734-6760.

[23] A. Palcic, B. Subotic, V. Valtchev, J. Bronic, *CrystEngComm* **2013**, *15*, 5784-5791.

[24] J. Aguado, D. P. Serrano, J. M. Escola, J. M. Rodrigez, *Microporous Mesoporous Mater.* **2004**, *75*, 41-49.

[25] Z. Qin, L. Lakiss, L. Tosheva, J.-P. Gilson, A. Vicente, C. Fernandez, V. Valtchev, *Adv. Funct. Mater.* **2014**, *24*, 257-264.

[26] K. S. Triantafyllidis, L. Nalbandian, P. N. Trikalitis, A. K. Ladavos, T. Mavromoustakos, C. P. Nicolaides, *Microporous Mesoporous Mater.* **2004**, *75*, 89-100.

[27] G. Majano, A. Darwiche, S. Mintova, V. Valtchev, *Ind. Eng. Chem. Res.* **2009**, *48*, 7084-7091.

[28] Y. Ni, A. Sun, X. Wua, G. Hai, J. Hua, T. Li, G. Li, *J. Coll. Inter. Sci.* **2011**, *361*, 521-526.

[29] F. Deng, Y. Yue, C. Ye, *Solid State Nucl. Magn. Reson.* **1998**, *10*, 151-160.

[30] C. P. Grey, A. J. Vega, *J. Am. Chem. Soc.* **1995**, *117*, 8232-8242.

[31] D. Massiot, F. Fayon, M. Capron, I. King, S. Le Calvé, B. Alonso, J. O. Durand, B. Bujoli, Z. Gan, G. Hoatson, *Magn. Reson. Chem.* **2002**, *40*, 70-76.

[32] S. Sklenak, J. Dedecek, C. Li, B. Wichterlova, V. Gabova, M. Sierka, J. Sauer, *Angew.*

Chem. Int. Ed. **2007**, *46*, 7286-7289.

[33] J. Dedecek, S. Sklenak, C. Li, B. Wichterlova, V. Gabova, J. Brus, M. Sierka, J. Sauer, *J. Phys. Chem. C* **2009**, *113*, 1447-1458.

[34] S. M. T. Almutairi, B. Mezari, G. A. Filonenko, P. C. M. M. Magusin, M. S. Rigutto, E. A. Pidko, E. J. M. Hensen, *ChemCatChem* **2013**, *5*, 452-466.

[35] A. Omegna, J. A van Bokhoven, R. Prins, *J. Phys. Chem. B* **2003**, *107*, 8854-8860.

[36] J. Jiao, J. Kanellopoulos, W. Wang, S. S. Ray, H. Foerster, D. Freude, M. Hunger, *Phys. Chem. Chem. Phys.* **2005**, *7*, 3221-3226.

[37] P. N. Kapoor, D. Heroux, R. S. Mulukutla, V. Zaikovskii, K. J. Klabunde, *J. Mater. Chem.* **2003**, *13*, 410-414.

[38] S. Jiansirisomboon, K. J. D. MacKenzie, S. G. Roberts, P. S. Grant, *J. Eur. Ceram. Soc.* **2003**, *23*, 961-976.

[39] Y. Mathieu, S. Rigolet, V. Valtchev, B. Lebeau, *J. Phys. Chem. C* **2008**, *112*, 18384-18392.

[40] T. H. Chen, B. H. Wouters, P. J. Grobet, *Eur. J. Inorg. Chem.* **2000**, 281-285.

[41] J. Chen, T. Chen, N. Guan, J. Wang, *Catal. Today* **2004**, *93-95*, 627-630.

[42] E. A. Pidko, S. M. T. Almutairi, B. Mezari, P. C. M. M. Magusin, E. J. M. Hensen, *ACS Catal.* **2013**, *3*, 1504-1517.

[43] J.-P. Gilson, G. Edwards, A. W. Peters, K. Rajagopalan, R. F. Wormsbecher, T. J. Roberie, M. P. Shatlock, *J. Chem. Soc. Chem. Commun.* **1987**, 91-92.

[44] P. Sazama, B. Wichterlova, J. Dedecek, Z. Tvaruzkova, Z .Musilova, L. Palumbo, S. Sklenak, O. Gonsiorova, *Microporous Mesoporous Mater* **2011**, *143*, 87-96.

[45] M. Smaihi, O. Barida, V. Valtchev, *Eur. J. Inorg. Chem.* **2003**, *24*, 4370-4377.

[46] M. V. Landau, D. Tavor, O. Regev, M. L. Kaliya, M. Herskowitz, V. Valtchev, S. Mintova, *Chem. Mater*. **1999**, *11*, 2030-2037.

[47] G. Engelhardt, D. Michel, High-resolution solid state NMR of silicates and zeolites, John Wiley & Sons, New York, **1987**.

[48] K. Barbera, F. Bonino, S. Bordiga, T. V. W. Janssen, P. Beato, *J. Catal.* **2011**, *280*, 196-205.

[49] Z. Qin, L. Lakiss, J.-P. Gilson, K. Thomas, J.-M. Goupil, C. Fernandez, V. Valtchev, *Chem. Mater.* **2013**, *25*, 2759-2766.

[50] M. Trombetta, T. Armaroli, A. Gutièrrez Alejandre, J. Ramirez Solis, G. Busca, *Appl. Catal.*

A **2000**, *192*, 125-136.

[51] I. Kiricsi, C. Flego, G. Pazzuconi, W. O. Parker Jr., R. Millini, C. Perego, G. Bellussi, *J. Phys. Chem* **1994**, *98*, 4627-4634.

[52] T. Armaroli, L. J. Simon, M. Digne, T. Montanari, M. Bevilacqua, V. Valtchev, J. Patarin, G. Busca, *Appl. Catal. A* **2006**, *306*, 78-84.

[53] F. Ngoye, L. Lakiss, Z. Qin, S. Laforge, C. Canaff, M. Tarighi, V. Valtchev, K. Thomas, A. Vicente, J.-P. Gilson, Y. Pouilloux, C. Fernandez, L. Pinard, *J. Catal.* **2014**, *320*, 118-126.

[54] C. Jia, P. Massiani, D. Barthomeuf, *J. Chem. Soc. Faraday Trans.* **1993**, *89*, 3659-3665.

[55] M. S. Holm, S. Svelle, F. Joensen, P. Beato, C. H. Christensen, S. Bordinga, M. Bjorgen, *Appl. Catal. A* **2009**, *356*, 23-39.

[56] S. Schallmoser, T. Ikuno, M. F. Wagenhofer, R. Kolvenbach, G. L. Haller, M. Sanchez-Sanchez, J. A. Lercher, *J. Catal.* **2014**, *316*, 93-102.

[57] T. C. Hoff, R. Thilakaratne, D. W. Gardner, R .C. Brown, J.-Ph. Tessonnier, *J. Phys. Chem. C* **2016**, *120*, 20103-20113.

[58] V. V. Ordomsky, V. Y. Murzin, Yu.V. Monakhova, Y. V. Zubavichus, E. E. Knyazeva, N. S. Nesterenko, I. I. Ivanova, *Microporous Mesoporous Mater.* **2007**, *105*, 101-110.

[59] M. Maache, A. Janin, J. C. Lavalley, J. F. Joly, E. Benazzi, *Zeolites* **1993**, *13*, 419-426.

[60] L. Lakiss, F. Ngoye, C. Canaff, S. Laforge, Y. Poullioux, Z. Qin, M. Tarighi, K. Thomas, V. Valtchev, A. Vicente, L. Pinard, J.-P. Gilson, C. Fernandez, *J. Catal.* **2015**, *328*, 165–172.

[61] X. Wu, S. Xu, W. Zhang, J. Huang, J. Li, B. Yu, Y. Wei, Z. Liu, *Angew. Chem. Int. Ed.* **2017**, *56*, 9039-9043.

[62] R. Khare, A. Bhan, *J. Catal.* **2015**, *329*, 218-228.

[63] D. Mores, J. Kornatowski, U. Olsbye, B. M. Weckhuysen, *Chem. Eur. J.* **2011**, *17*, 2874-2884.

[64] S. Müller, Y. Liu, M. Vishnuvarthan, X. Sun, A. C. van Veen, G. L. Haller, M. Sanchez-Sanchez, J. A. Lercher, *J. Catal.* **2015**, *325*, 48-59.

[65] X. Sun, S. Mueller, Y. Liu, H. Shi, G. L. Haller, M. Sanchez-Sanchez, A. C. van Veen, J. A. Lercher, *J. Catal.* **2014**, *317*, 185-197.

[66] J. Meusinger, A. Corma, *J. Catal.* **1996**, *159*, 353-360.

[67] A. Comas-Vives, M. Valla, C. Copéret, P. Sautet, *ACS Cent. Sci.* **2015**, *1*, 313-319.

1   [68] C. A. Emeis, *J. Catal.* **1993**, *141*, 347-354.

2   [69] T. Onfroy, G. Clet, M. Houalla, *Microporous Mesoporous Mater.* **2005**, *82*, 99-104.